nature communications

Article

https://doi.org/10.1038/s41467-024-54277-z

Transforming carbon dioxide into a methanol surrogate using modular transition metal-free Zintl ions

Received: 1 July 2024

Accepted: 5 November 2024

Published online: 19 November 2024

Check for updates

Bono van IJzendoorn[1], Saad F. Albawardi[1], William D. Jobbins[2], George F. S. Whitehead[2], John E. McGrady[1] ✉ & Meera Mehta[1] ✉

Although not the only greenhouse gas, CO_2 is the poster child. Unsurprisingly, therefore, there is global interest across industrial and academic research in its removal and subsequent valorisation, including to methanol and its surrogates. Although difficult to study, the heterogenous pnictogens represent one important category of catalytic materials for these conversions; their high crustal abundance and low cost offers advantages in terms of sustainability. Here, Zintl clusters based on these elements are studied as homogenous atom-precise models in CO_2 reduction. A family of group 13 functionalized pnictogen clusters with the general formula $[(R_2E)Pn_7]^{2-}$ (E = B, Al, In; Pn = P, As) is synthesized and their catalytic competency in the reduction of CO_2 probed. Trends in both turnover numbers and frequencies are compared across this series, and $[(i\mathrm{Bu}_2\mathrm{Al})P_7]^{2-}$ found to be very high-performing and recyclable. Electronic structures across the series are compared using density functional theory to provide mechanistic insights.

Carbon dioxide (CO_2) is perhaps the most notorious and well-recognized greenhouse gas. Its reputation is well earned, as there has been almost a 50% increase in atmospheric CO_2 since the industrial revolution, which is directly linked to global warming, associated natural disasters, rising sea levels and ice sheet degradation[1–3]. This increase in atmospheric carbon is a direct result of global energy dependence on fossil fuel combustion. Methanol (CH_3OH) is one alternative clean fuel source, as well as a basic C1 building block for the molecules that underpin everyday life, from pharmaceuticals and agrochemicals to adhesives, paints and coatings[4,5]. Globally, 140 million metric tonnes of CH_3OH were consumed in 2018, and this demand is expected to double by 2030[6]. Strategies that recycle CO_2 directly into methanol (or its surrogates), which can then be burned for energy or used as industry feedstocks, offer the possibility of closing the carbon cycle[3,7–10], and it is therefore no surprise that facilitating this transformation is of great global interest. However, the high thermodynamic stability of CO_2 means that technologies that mediate its transformation often rely on catalysts featuring transition metals, including those that fall in the Platinum Group[11–16]. The high cost of these metals is an obvious impediment to their widespread application, and inexpensive and sustainable alternatives are an important target[7].

One possible approach to minimize costs is to replace the expensive transition metal catalysts with inexpensive ones based on earth-abundant elements[17–20], where systems based on heterogenous phosphorus are of increasing interest[21–24]. Although their structures are not yet fully understood, red and violet phosphorus contain clusters of phosphorus between four and nine units that are polymerized and crosslinked together[25–27]. Heterogenous catalysts are often more robust and easier to separate compared to homogenous systems, minimizing purification costs and enabling catalyst recycling[28]. In situ mechanistic insights will be essential to release the full catalytic potential of materials based on heterogenous phosphorus, but these studies are extremely difficult to perform due to their extreme insolubility. In this context, Zintl clusters based on the $[P_7]$ architecture offer an alternative source of mechanistic insight. Clusters of this type can be considered as intermediates between mono-nuclear phosphorus species and bulk solids, and they have the advantage of being

[1]Department of Chemistry, University of Oxford, 12 Mansfield Road, Oxford OX1 3QR, UK. [2]Department of Chemistry, University of Manchester, Oxford Road, Manchester M13 9PL, UK. ✉e-mail: John.mcgrady@chem.ox.ac.uk; Meera.mehta@chem.ox.ac.uk

easily synthetically accessible, soluble in common solvents, and they provide convenient spectroscopic handles to probe reactivity. A detailed understanding of catalytic activity of [P_7] clusters may, therefore, offer a window into the analogous chemistry with heterogenous phosphorus.

The application of Zintl clusters as components in catalyst design is a new field[29], and in most of the previous reports, the clusters act as innocent ligands that support catalytically active transition metals (Fig. 1). For example, Goicoechea and Weller have coordinated [Ge_9] to Rh metal and mediated the hydrogenation of olefins, and then later used the same system in H/D exchange reactions (Fig. 1)[30,31]. Fässler and co-workers have also employed a [Ge_9] cluster, in this case with Ni coordinated to mediate alkene isomerization[32]. Although not derived from a Zintl species, Scheschkewitz and co-workers also facilitated alkene isomerization with a silicon-iridium cluster system[33]. Sun and co-workers used Ru encapsulated by a Sn cluster dispersed on a CeO_2 surface to affect the reverse water-gas shift reaction[34], although the extent to which the cluster remains intact after dispersion is still unclear.

In 2022, we reported that the transition metal-free boron-functionalized [P_7] cluster [κ^2-(BBN)P_7]$^{2-}$ ([**1**]$^{2-}$; BBN = 9-borabicyclo[3.3.1]nonane) was catalytically competent for the hydroborative reduction of C=O bonds in carbonyls and CO_2, as well as the C=N bonds in isocyanates, carbodiimides, imines, pyridines and nitriles[35,36]. In this paper, we extend that work by preparing a wider family of group 13 functionalized heptapnictogen clusters with the general formula [κ^2-(R_2E)Pn_7]$^{2-}$ (E = B, Al, In, Pn = P, As). Whilst the [κ^2-(Ph_2In)P_7]$^{2-}$ cluster has previously been prepared by the Goicoechea group[37], the synthesis of clusters [κ^2-(*i*Bu_2Al)P_7]$^{2-}$ and [κ^2-(*i*Bu_2Al)As_7]$^{2-}$ are reported here. We compare the catalytic performance of this series in the hydroborative reduction of CO_2 gas with respect to selectivity, turnover number (TON), and turnover frequency (TOF), and show that this family of catalysts are highly competent with the aluminium species being the most active. By systematically modifying catalyst design, we are able to better understand their reactivity landscape, and in this work, the identity of the group 13 moiety is found to have a major impact on reactivity. Our mechanistic studies further allowed us to uncover a catalytic off-cycle intermediate, and consider an alternative mechanism for this transformation. Additionally high catalyst recyclability is proven, an added advantage of employing systems based on functionalized [Pn_7] clusters.

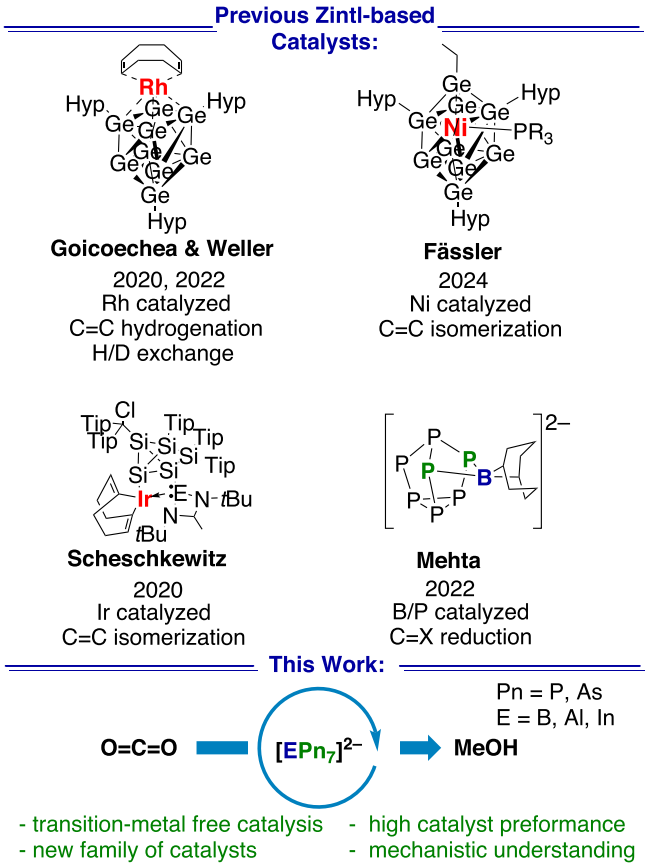

Fig. 1 | Select examples of Zintl clusters that have been applied in homogenous catalysis, and this work. Hyp = Si(SiMe$_3$)$_3$, Tip = 2,4,6-triisopropylphenyl, E = Si, Ge, or Sn.

Results and discussion

Synthesis and properties of [κ^2-(R_2E)Pn_7]$^{2-}$ clusters

The [κ^2-(*i*Bu_2Al)Pn]$^{2-}$ (Pn = P ([**2**]$^{2-}$), As ([**3**]$^{2-}$)) clusters were synthesised using protocols analogous to [κ^2-(BBN)P_7]$^{2-}$ ([**1**]$^{2-}$)[35]; specifically diisobutylaluminium hydride was dehydrocoupled with the protonated clusters [HPn_7]$^{2-}$ (Pn = P, As)[38,39], leading to H_2 gas evolution (Fig. 2a). In line with the nuclear magnetic resonance (NMR) spectroscopic features reported for [κ^2-(R_2E)P_7]$^{2-}$ (R_2E = BBN, Ph_2In)[35,37], the [κ^2-(*i*Bu_2Al)P_7]$^{2-}$ cluster reveals five resonances in the ^{31}P NMR spectrum consistent with κ^2-coordination to the [P_7] core. Multiple efforts were made to acquire a ^{27}Al NMR spectrum to establish the coordination mode of Al to the phosphorus cluster, but with no success. The synthesis of the related [κ^2-((Me_2N)$_2$Ga)P_7]$^{2-}$ was also investigated by reacting (Me_2N)$_3$Ga dimer with [HP_7]$^{2-}$ and resulted in ^{31}P NMR spectra consistent with the formation of the expected product. However, despite multiple efforts isolation of analytically pure material was not achieved and precluded further catalytic investigations (see Supplementary Information section 2.3).

Single crystals were acquired for both the [Na(18c6)]$_2$[**2**] and [K(18c6)]$_2$[**3**] (18c6 = 18-crown-6) salts and X-ray diffraction (XRD) studies confirmed the κ^2-coordination mode of the Al to the [Pn_7] core, see Fig. 2b, c. The bond metric data obtained by the XRD analysis allows for direct comparison between the [κ^2-(*i*Bu_2Al)Pn_7]$^{2-}$ clusters, and hence, the influence of the [Pn_7] core on the substitution. Firstly, as expected, the average Al–P bonds in [**2**]$^{2-}$ (2.4429(14) Å) are shorter compared to the average Al–As bonds in [**3**]$^{2-}$ (2.528(19) Å) due to the larger atomic radius of As compared to P[40]. Also consistent with the atomic size difference between phosphorus and arsenic, the P–Al–P bond angle in [**2**]$^{2-}$ is more acute (84.46(3)°) when compared to the As–Al–As bond angle in [**3**]$^{2-}$ (89.2(4)°). The bond distances within the [Pn_7] cores are similar to those in the unfunctionalized [Pn_7]$^{3-}$ clusters, and differences are again consistent with the differences in atomic radius of As and P[41]. Meaningful comparisons can also be made between the family of group 13 functionalized phosphorus clusters [κ^2-(R_2E)P_7]$^{2-}$ (E = B, Al, In) clusters[35,37], where the average E–P bond lengths increase down the group (B–P: 2.067(11) Å in [**1**]$^{2-}$; Al–P: 2.4429(14) Å in [**2**]$^{2-}$; In–P: 2.578(2) Å in [**4**]$^{2-}$). Further, the P–E–P bond angles become more acute for the heavier group 13 elements (P–B–P: 93.3(3)° in [**1**]$^{2-}$, P–Al–P: 84.46(3)° in [**2**]$^{2-}$, P–In–P: 80.33(4)° in [**4**]$^{2-}$): presumably this changing bond angle reflects the approximately constant bite angle of the P_7 unit leading to more acute angles as the bonds get longer.

Catalytic reduction of carbon dioxide

We have previously reported a detailed study of the catalytic reduction of carbonyl functional groups using [**1**]$^{2-}$[35], and clusters [**2**]$^{2-}$ to [**4**]$^{2-}$ all showed similar reactivity towards acetophenone and benzaldehyde that is consistent with activation of the unsaturated C=O bond (see Supplementary Information section 4.1). Motivated by this observation, the catalytic competence of the family of clusters [κ^2-(R_2E)Pn_7]$^{2-}$ (E = B, Al, In, Pn = P, As) ([**1**]$^{2-}$- [**4**]$^{2-}$) towards the hydroborative reduction of CO_2 was probed using the previously reported optimised conditions: 1 atm of CO_2, 0.33 % catalyst loading; room temperature

https://doi.org/10.1038/s41467-024-54277-z

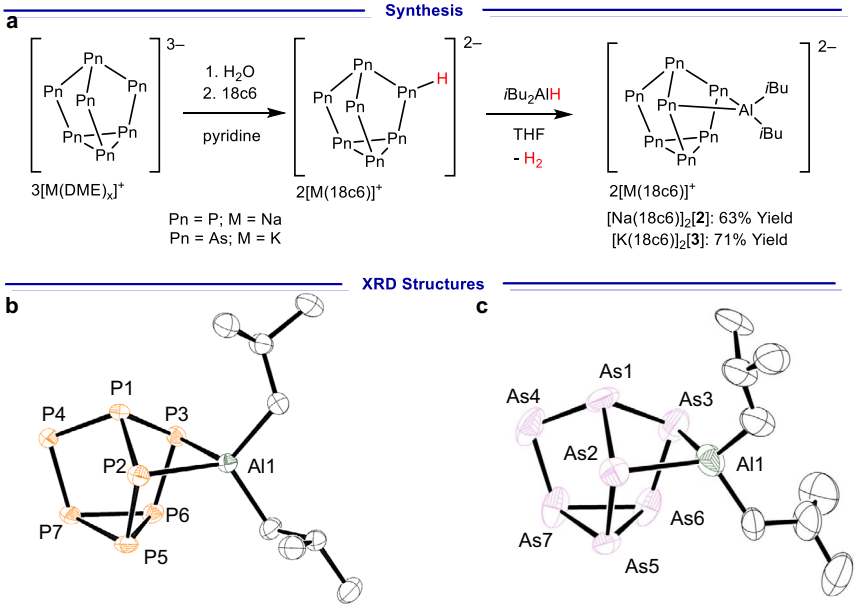

Fig. 2 | Synthesis and X-ray diffraction structures of [Na(18c6)]$_2$[2] and [K(18c6)]$_2$[3]. **a** Synthesis of [Na(18c6)]$_2$[**2**] and [K(18c6)]$_2$[**3**]. 18c6 = 18-crown-6. **b** Molecular structure of [κ^2-(*i*Bu$_2$Al)P$_7$]$^{2-}$ ([**2**]$^{2-}$) in the [Na(18c6)]$_2$[(*i*Bu$_2$Al)P$_7$] salt. Anisotropic displacement ellipsoids pictured at 50% probability. Hydrogen atoms, and [Na(18c6)]$^+$ counter cations omitted for clarity. Phosphorus: orange; aluminium: green; carbon: white. Selected bond lengths [Å]: Al1–P2 2.4385(10), Al1–P3 2.4472(10), P1–P2 2.127(10), P1–P3 2.1877(10), P1–P4 2.1592(10), P2–P5 2.1809(10), P3–P6 2.1807(10), P4–P7 2.1433(10), P5–P6 2.2589(11), P5–P7 2.2346(10), P6–P7 2.2338(10); selected bond angle [°]: P2–Al1–P3 84.46(3). **c** Molecular structure of [κ^2-(*i*Bu$_2$Al)As$_7$]$^{2-}$ ([**3**]$^{2-}$) in the [K(18c6)]$_2$[(*i*Bu$_2$Al)As$_7$] salt, two. Anisotropic displacement ellipsoids pictured at 50% probability. Hydrogen atoms, and [K(18c6)]$^+$ counter cations omitted for clarity. Arsenic: plum; aluminium: green; carbon: white. Selected bond lengths [Å]: Al1–As2 2.513(9), Al1–As3 2.529(9), As1–As2 2.460(5), As1–As3 2.423(4), As1–As4 2.352(5), As2–As5 2.383(4), As3–As6 2.380(4), As4–As7 2.340(6), As5–As6 2.469(4), As5–As7 2.467(6), As6–As7 2.464(4); selected bond angle [°]: As2–Al1–As3 89.7(3).

(RT); 18 h; *o*-difluorobenzene (*o*DFB):toluene (Tol) solvent system; and HBBN dimer as the reductant. The findings are summarized below in Table 1. We note that we were only able to prepare the Na$^+$ salt of [**2**]$^{2-}$ and the K$^+$ salt of [**3**]$^{2-}$. However, for [**4**]$^{2-}$, where both the Na$^+$ and K$^+$ salts could be prepared, and there is no discernible difference in TOF$_{RT}$. This observation is fully consistent with our previous findings for [κ^2-(BBN)P$_7$]$^{2-}$ ([**1**]$^{2-}$) where both the Na and K salts were also tested[35], and suggests that the identity of the s-block cation does not influence catalytic performance to any great extent. Isotopic labelled studies using ^{13}C-labelled CO_2 confirmed the origin of the carbon products (see Supplementary Information section 3.2.).

Taking the catalytic performance of [Na(18c6]$_2$[**1**] as a baseline (TOF$_{RT}$ = 30 h^{-1}, TOF$_{50\,°C}$ = 300 h^{-1}, 99% selectivity for MeOBBN [a methanol surrogate which can be quantitatively and easily hydrolyzed to methanol[35]]), the aluminium-functionalized cluster [**2**]$^{2-}$ displayed greater reactivity at 0.33 mol% loading both at RT (TOF$_{RT}$ = 38 h^{-1}) and at 50 °C (TOF$_{50\,°C}$ = 577 h^{-1}). The TOF$_{50\,°C}$ for the Al cluster [**2**]$^{2-}$ is almost twice that of the boron cluster [**1**]$^{2-}$, but the selectivity decreases to 65% MeOBBN, with the remaining 34% of product being the diol surrogate $CH_2(OBBN)_2$. Selectivity towards MeOBBN can be recovered by reducing the catalyst loading from 0.33 mol% to 0.10 mol % at RT without any great impact on TOF$_{RT}$ (42 h^{-1}). For the As analogue, [κ^2-(*i*Bu$_2$Al)As$_7$]$^{2-}$ ([**3**]$^{2-}$), slightly higher TOFs are observed at 0.33 mol% loading when compared to the [κ^2-(BBN)P$_7$]$^{2-}$ ([**1**]$^{2-}$) (TOF$_{RT}$ = 33 h^{-1} and TOF$_{50\,°C}$ = 361 h^{-1}). The selectivity towards MeOBBN is again lower than for [κ^2-(BBN)P$_7$]$^{2-}$ ([**1**]$^{2-}$), and again it can be increased by reducing the catalyst loading to 0.10 mol% with no significant impact on TOF$_{RT}$ (34 h^{-1}). The indium-functionalized cluster [κ^2-(Ph$_2$In)P$_7$]$^{2-}$ ([**4**]$^{2-}$) was found to have poorer catalytic performance when compared to the other [κ^2-(R$_2$E)Pn$_7$]$^{2-}$ systems investigated here, with maximum TOF$_{RT}$ of 13 h^{-1} and TOF$_{50\,°C}$ of 156 h^{-1}. As measured by TOF, the catalytic performance across the entire series decreases in the order: [κ^2-(*i*Bu$_2$Al)P$_7$]$^{2-}$ > [κ^2-(*i*Bu$_2$Al)As$_7$]$^{2-}$ > [κ^2-(BBN)P$_7$]$^{2-}$ > [κ^2-(Ph$_2$In)P$_7$]$^{2-}$.

In order to probe the origins of the lower selectivity of [**2**]$^{2-}$ and [**3**]$^{2-}$ for MeOBBN compared to [**1**]$^{2-}$, the reaction mixtures were monitored by ^{1}H NMR spectroscopy. The reaction profiles for the hydroboration of CO_2 using 0.33 mol% [κ^2-(*i*Bu$_2$Al)P$_7$]$^{2-}$ or [κ^2-(*i*Bu$_2$Al)As$_7$]$^{2-}$ as catalyst at RT are given in Supplementary Information Figs. S14 and S15, and both show initial rapid formation of $CH_2(OBBN)_2$ which then decays over time to form MeOBBN. Unlike the corresponding reaction profiles, we previously reported for catalyst [**1**]$^{2-}$[35], not all the $CH_2(OBBN)_2$ is fully consumed before the remaining HBBN dimer has all reacted (observed by ^{1}H NMR spectroscopy). Neither the carboxyl-BBN (HC(=O)OBBN) nor formaldehyde is observed under these conditions, in line with literature reports where it is believed that the susceptibility towards hydroboration follows the order HC(=O)OBBN > CO_2 > $CH_2(OBBN)_2$ > MeOBBN, with HC(=O)OBBN being the most reactive[42]. We propose that the more polarized Al–Pn (Pn = P, As) bonds (when compared to the B–P bonds), in combination with the relatively high oxophilicity and electropositivity of Al compared to other group 13 elements[43], makes catalysts [**2**]$^{2-}$ and [**3**]$^{2-}$ more prone to CO_2 capture. As CO_2 hydroboration to MeOBBN requires three hydroboration steps, activation of a new molecule of CO_2 competes with activation of a previously hydroborated $CH_2(OBBN)_2$ molecule for re-entry into the catalytic cycle. We also noticed that selectivity for MeOBBN increases at lower catalyst loadings; we believe this is related to the amount of catalytic material at the solution-gas interface, where the concentration of CO_2 is highest. To test this concept, a dilution experiment was conducted where catalyst loading relative to borane was held constant, but an overall increase in solvent would also result in less catalytic material at the solvent-atmosphere interface (see Supplementary Information section 3.3.2). In Table 1 the 0.33 mol% catalyst loading [κ^2-(*i*Bu$_2$Al)P$_7$]$^{2-}$ reaction at RT was performed at 1.94 mM catalyst concentration and resulted in a 35:65 product distribution of $CH_2(OBBN)_2$:MeOBBN, but dilution to 0.97 mM catalyst concentration now resulted in a 25:75 product distribution. Another approach to change the amount of catalytic material at the solution-

https://doi.org/10.1038/s41467-024-54277-z

Table 1 | Hydroboration of CO_2 by $[\kappa^2\text{-}(R_2E)Pn_7]^{2-}$ clusters

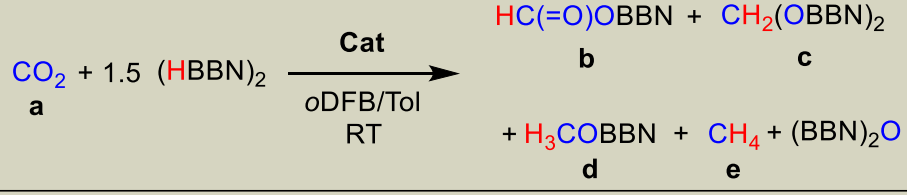

Cat	Loading (%)[a]	Time (h)	Temp. (°C)	b Conv. (%)[b]	c Conv. (%)[b]	d Conv. (%)[b]	e Conv. (%)[b]	TOF (h^{-1})[b]
$[K(18c6)]_2$ [**1**][35]	0.33	10	RT	0	0	>99	0	30
$[Na(18c6)]_2$ [**1**][35]	0.33	10	RT	0	0	>99	0	30
	0.33	1	50	0	0	>99	0	300
	0.10	32	RT	0	0	>99	0	31
$[Na(18c6)]_2$ [**2**]	0.33	8	RT	0	34	65	0	38
	0.33	0.52	50	0	34	65	0	577
	0.10	24	RT	0	0	>99	0	42
$[K(18c6)]_2$ [**3**]	0.33	9.1	RT	0	30	69	0	33
	0.33	0.83	50	0	29	70	0	361
	0.10	30	RT	0	0	>99	0	34
$[K(18c6)]_2$ [**4**]	0.33	24	RT	0	0	>99	0	13
$[Na(18c6)]_2$ [**4**]	0.33	24	RT	0	0	>99	0	13
	0.33	1.92	50	0	10	89	0	156
	0.10	120	RT	0	0	98	0	8

[a]Relative to B–H bonds.
[b]Determined by ^{1}H NMR spectroscopy, based on C–H bond formation using hexamethylbenzene as an internal standard.

gas interface, would be to change the diameter (⌀) of the reaction vessel (see Supplementary Information section 3.3.2). To this end, when the hydroboration of CO_2 (0.33 mol% loading $[\kappa^2\text{-}(i\text{Bu}_2\text{Al})\text{P}_7]^{2-}$, RT) was repeated again at 1.94 mM concentration but performed in a J Young ampoule (⌀ = 30 mm) instead of in a J Young NMR tube (⌀ = 5 mm) the ratio of products was found to be 63:37 $CH_2(OBBN)_2$:MeOBBN product distribution. Both of these experiments are consistent with the local concentration of catalyst at the solution-gas interface having an impact on product selectivity, where less catalytic material correlates to greater MeOBBN selectivity.

Since catalyst $[Na(18c6)]_2[\kappa^2\text{-}(i\text{Bu}_2\text{Al})\text{P}_7]$ ($[Na(18c6)]_2$[**2**]) was found to be the most active in terms of TOF, efforts were made to optimize the reaction conditions to select for the formation of MeOBBN (Table 2). High catalyst loadings of 10% and 1% (entries 1 and 2) showed low selectivity for MeOBBN, with only approximately 50% conversion. Further, at 10 mol% catalyst loading crystals of $[Na(18c6)][(HCO_2)_2\text{BBN}]$ (compound **28b'** in ref. 35) could be collected[35]. In the previous discussion of the data in Table 1 we demonstrated that reducing the catalyst loading to 0.1 mol% at RT increases selectivity, with MeOBBN then being observed as the sole product. In an effort to increase TOF, 0.1 mol% catalyst loading of $[\mathbf{2}]^{2-}$ was investigated at 50, 60 and 70 °C (entries 3–5) but, in these cases, selectivity towards MeOBBN decreased and at 70 °C overall conversion also decreased. Heating of $[Na(18c6)]_2[\kappa^2\text{-}(i\text{Bu}_2\text{Al})\text{P}_7]$ revealed rapid catalyst decomposition at 70 °C, slower decomposition at 60 °C, and no decomposition at 50 °C, as measured by ^{31}P NMR spectroscopy (see Supplementary Information section 3.3.3). Lowering the catalyst loading further to 0.05 mol% at RT (entry 6) revealed a decrease in TOF_{RT} while retaining high selectivity and a high TON of 2000. Increasing the temperature with 0.05 mol% loading (entries 7–9), again decreased selectivity. Lowering the loading even further to 0.01 mol%, (entries 10 and 11) gave the highest TONs of 9400 and 9600 at RT and 50 °C, respectively. For $[Na(18c6)]_2[\kappa^2\text{-}(i\text{Bu}_2\text{Al})\text{P}_7]$ ($[Na(18c6)]_2$[**2**]) a maximum TOF of 741 h^{-1} considering all products and 600 h^{-1} considering only MeOBBN was obtained. Analysis of these TON and TOFs reveal that $[Na(18c6)]_2[\kappa^2\text{-}(i\text{Bu}_2\text{Al})\text{P}_7]$ ($[Na(18c6)]_2$[**2**]) outperforms our previously reported boron-functionalized analogue $[\mathbf{1}]^{2-}$ in its ability to mediate this transformation, and in fact, it is highly competitive with other main group catalysts and even many homogenous transition metal catalysts (see Supplementary Information sections 3.6. and 3.7.).

Recycling

Previously, we reported that $[Na(18c6)]_2[\kappa^2\text{-}(\text{BBN})\text{P}_7]$ ($[Na(18c6)]_2$[**1**]) could be recycled 7 times in the catalytic hydroboration of CO_2 with no loss in performance[35]. To investigate the recyclability of the $[Na(18c6)]_2[\kappa^2\text{-}(i\text{Bu}_2\text{Al})\text{P}_7]$ ($[Na(18c6)]_2$[**2**]) catalyst, the hydroboration of CO_2 was performed using 0.1 mol% loading at RT and after complete conversion investigation by ^{31}P NMR spectroscopy revealed that the catalyst was still present (see Supplementary Information Fig. S29). Furthermore, minimal changes in catalytic competency were observed after reloading the reaction mixture with HBBN dimer and CO_2 9 times, indicating living catalysis (see Fig. 3). After these cycles, the catalyst was recovered from the reaction mixture and re-used in an independent reaction batch (cycle 11 Fig. 3), and again no decrease in catalytic performance was observed. Overall these experiments show that the $[Na(18c6)]_2[\kappa^2\text{-}(i\text{Bu}_2\text{Al})\text{P}_7]$ ($[Na(18c6)]_2$[**2**]) catalyst is very robust with a total of 3.18 mmol MeOBBN being produced from 0.3 μmol $[\mathbf{2}]^{2-}$, a 10778-fold excess. This type of high recyclability amongst homogenous catalysts is uncommon, and highlights one of the advantages of building systems based on the $[Pn_7]$ framework.

Mechanistic investigations

Benzaldehyde was used as a model substrate to investigate the kinetics of hydroboration as it can be easily weighed into the reaction mixture and, unlike gaseous CO_2, primarily resides in the solution phase with the other reagents. Mimicking conditions used in the hydroboration of CO_2 (0.1 mol% loading, RT, 1:1 *o*DFB:Tol), variable time normalization analysis was applied to probe the order of the reagents (data regarding VTNA analysis available in Supplementary Data 2). Both the $[Na(18c6)]_2$[**1**] and $[Na(18c6)]_2$[**2**] catalysts were investigated following the VTNA method described by the Burés group (see Supplementary Information section 5), where the reaction order can be obtained via a graphical representation[44,45]. For both $[Na(18c6)]_2$[**1**] and $[Na(18c6)]_2$[**2**] catalysts using HBBN dimer as reductant, the analysis supports a fitting of a zero-order in the concentration of aldehyde and catalyst and a half-order in the concentration of HBBN dimer. This suggests that the rate limiting step is a reaction involving HBBN dimer but not the catalysts, therefore we propose the breaking of the HBBN dimer is rate limiting. When changing the reductant from HBBN dimer to the monomeric HBpin, the analysis supports a fitting of a zero-order in the concentration of aldehyde and the first order in the concentration of borane and in the concentration of catalysts. These findings suggest a fast activation of the C=O bond and slow activation of the B–H bond, consistent with the observed stoichiometric reactivity discussed below. To further investigate the potential rate-determining step, kinetic isotope effects were probed by performing the hydroboration of benzaldehyde with DBpin (0.1 mol% loading, RT). The initial rate from the DBpin reaction was determined and compared to the initial rate of the analogous reaction with HBpin. A kinetic isotope effect (K_H/K_D) was found at 2.16, a value that is in good agreement with other hydroboration catalysts where B–H activation or hydride transfer is presumed to be one of the slow steps[46–48].

In our previous report on the catalytic hydroboration of CO_2 by $[Na(18c6)]_2[\kappa^2\text{-}(\text{BBN})\text{P}_7]$ ($[Na(18c6)]_2$[**1**]), we also performed a complementary series of 1:1 stoichiometric reactions with a range of unsaturated molecules including benzaldehyde, acetophenone and phenyl isocyanate, and also with the boranes HBpin and HBBN dimer[35]. In that study, we noted that $[Na(18c6)]_2[\kappa^2\text{-}(\text{BBN})\text{P}_7]$ reacts rapidly with C=O bonds but rather more slowly with B–H bonds. Here, the corresponding reactivity of the Al analogue $[Na(18c6)]_2[\kappa^2\text{-}(i\text{Bu}_2\text{Al})\text{P}_7]$ ($[Na(18c6)]_2$[**2**]) towards the same set of substrates is probed. A 1:1 reaction of $[Na(18c6)]_2$[**2**] with HBpin at RT revealed no reaction (monitored using ^{11}B and ^{31}P NMR spectroscopy), precisely as was observed for $[Na(18c6)]_2$[**1**]. However, when the HBBN dimer was used in place of HBpin, a new cluster was identified after 10 hours with ^{11}B and ^{31}P NMR resonances that are consistent with the insertion of HBBN into one of the Al–P bonds of $[Na(18c6)]_2$[**2**]. In contrast, the stoichiometric reaction of $[Na(18c6)]_2$[**2**] with benzaldehyde at RT revealed almost immediate formation of two other clusters by ^{31}P NMR spectroscopy, along with some unreacted $[Na(18c6)]_2$[**2**] (Fig. 4a). Addition of a second equivalent of benzaldehyde drove the reaction further, such that only one of the two products is observed. The ^{31}P NMR spectrum of the final product has five peaks in a 2:1:1:1:2 integral ratio, consistent with a symmetric $[P_7]$ cluster system with a mirror plane, similar to $[Na(18c6)]_2$[**2**] itself. On that basis, the two new clusters are proposed to be the mono-inserted benzaldehyde ($[\kappa^2\text{-}(i\text{Bu}_2\text{Al-O(Ph)(H)C)P}_7]^{2-}$, $[\mathbf{5}]^{2-}$) and bis-inserted benzaldehyde ($[\kappa^2\text{-}(i\text{Bu}_2\text{Al-(O(Ph)(H)C)}_2\text{)P}_7]^{2-}$, $[\mathbf{6}]^{2-}$) products shown in Fig. 4a. ^{1}H NMR, ^{13}C NMR, ^{31}P COSY NMR, and ^{1}H^{13}C HSQC (Heteronuclear Single Quantum Coherence) NMR spectroscopic studies are fully consistent with this proposal (see Supplementary Information section 4.1.3). When the starting material $[\mathbf{2}]^{2-}$ was added to a reaction mixture containing only the bis-inserted product $[\mathbf{6}]^{2-}$, over several hours, the mono-inserted product $[\mathbf{5}]^{2-}$ was detected by ^{31}P NMR spectroscopy, consistent with an equilibrium between $[\mathbf{5}]^{2-}$ and $[\mathbf{6}]^{2-}$. If the bulkier acetophenone is used in place of benzaldehyde, only the mono-inserted ($[\kappa^2\text{-}(i\text{Bu}_2\text{Al-O(Ph)(Me)C)P}_7]^{2-}$, $[\mathbf{7}]^{2-}$) is observed: no evidence for the bis-inserted product was detected by ^{31}P NMR spectroscopy. The mono-inserted products have a distinctive 7 resonance pattern in the ^{31}P NMR spectrum, and the most downfield chemical shift (^{31}P δ: 115 ppm) is similar

https://doi.org/10.1038/s41467-024-54277-z

Table 2 | Hydroboration of CO_2 with catalyst $[2]^{2-}$

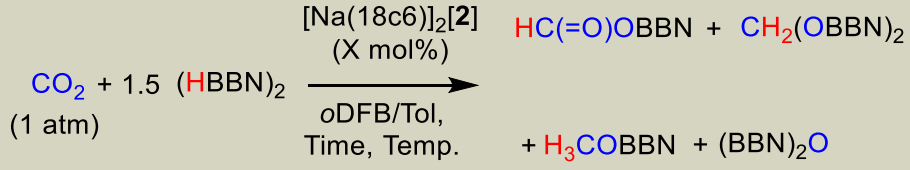

Entry	$[Na(18c6)]_2[2]$ (mol %)[a]	Time (h)	T (°C)	MeOBBN Conv. (%)[b]	$CH_2(OBBN)_2$ Conv. (%)[b]	TON [c]	TOF (h^{-1}) [c]
1	10	1	RT	51	0	5	5
2	1.0	3	RT	58	39	97(58)	33(19)
3	0.10	1.75	50	80	19	1000(800)	571(457)
4	0.10	1.35	60	81	18	1000(810)	741(600)
5	0.10	2	70	50	5	550(500)	224(250)
6	0.05	72	RT	>99	0	2000	28
7	0.05	7.5	40	50	25	1500 (1000)	200(133)
8	0.05	4.3	50	80	19	2000 (1600)	465(372)
9	0.05	3	60	80	2	1760 (1600)	586(533)
10	0.01	400	RT	94	0	9400	24
11	0.01	66	50	96	0	9600	145

No carboxyl-borane or methane formation was observed by ^{1}H NMR spectroscopy.

[a]Relative to B–H bonds.

[b]Determined by ^{1}H NMR spectroscopy, based on C–H bond formation using hexamethylbenzene as an internal standard.

[c]TON and TOF considering only MeOBBN formation given in parentheses.

https://doi.org/10.1038/s41467-024-54277-z

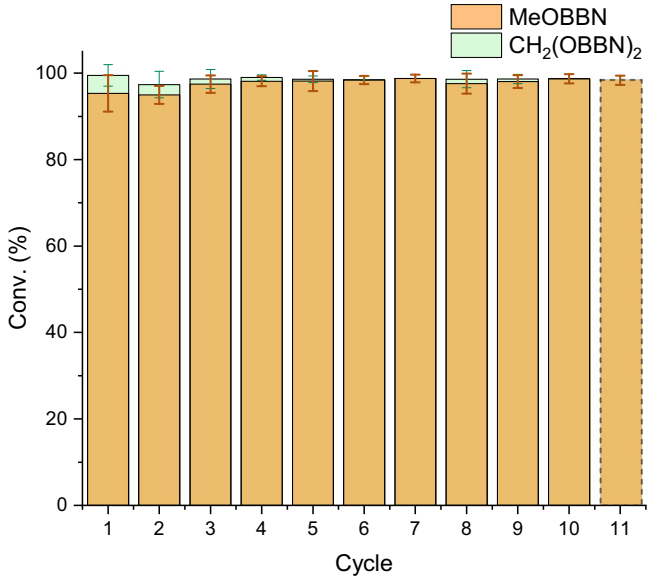

Fig. 3 | Catalyst recycling in the hydroboration of CO_2 using 0.1 mol% loading [Na(18c6)]$_2$[2]. Cycle 11 is after the catalyst was recovered from cycle 10 and added to a fresh batch of the reaction. Error bars indicate the 95% confidence interval.

to other P–C carbonyl functionalized clusters[49,50], indicating [P_7]–C bond formation. The formation of the bis-inserted product may be precluded with increasing steric bulk at the carbonyl. It is worth noting here that in the case of CO_2 activation, steric bulk is minimal, and thus, bis-insertion to give structures analogous to [**6**]$^{2-}$ should be possible.

Stoichiometric reductions of benzaldehyde were then performed using [Na(18c6)]$_2$[κ^2-(*i*Bu$_2$Al)P$_7$] ([Na(18c6)]$_2$[**2**]) and HBpin as the hydride source (Fig. 4c). Initially, [Na(18c6)]$_2$[**2**] was allowed to react with 1 equivalent of benzaldehyde, as described above, and subsequently 1 equivalent of HBpin was added; the Bpin-hydroborated product was obtained in 8% yield, and no transfer of the *i*Bu$_2$Al-unit to the carbonyl was observed. ^{31}P NMR spectroscopy confirmed the presence of [**5**]$^{2-}$ and [**6**]$^{2-}$ in the reaction mixture with small residual amounts of [**2**]$^{2-}$. The order in which the reagents are added has a strong influence on the yield; if the order of addition is reversed so that we add 1 equivalent HBpin first to [Na(18c6)]$_2$[κ^2-(*i*Bu$_2$Al)P$_7$] followed by addition of 1 equivalent benzaldehyde, the hydroborated product is generated in 58% yield. ^{31}P NMR spectra show, in this case, that the dominant species in solution is [**2**]$^{2-}$ with only minor amounts [**5**]$^{2-}$ and [**6**]$^{2-}$. These observations are consistent with the formation of the bis-inserted [**6**]$^{2-}$ product being an off-cycle thermodynamic sink which inhibits the formation of hydroborated product. However, when the reductant is present, hydroboration of the C=O bond competes with the formation of the bis-inserted product, and thus, the hydroborated product is observed in higher yield. Related reactions were also conducted with [Na(18c6)]$_2$[κ^2-(BBN)P$_7$] ([Na(18c6)]$_2$[**1**]), [K(18c6)]$_2$[κ^2-(*i*Bu$_2$Al)As$_7$] ([K(18c6)]$_2$[**3**]) and [Na(18c6)]$_2$[κ^2-(Ph$_2$In)P$_7$] ([Na(18c6)]$_2$[**4**]), and again it was found that the order of addition influenced the observed conversion to hydroborated product with the difference being significantly less pronounced for [**4**]$^{2-}$ (Fig. 4b–e). In our previous work, when [**1**]$^{2-}$ was studied in a related reaction with acetophenone it was found that there is a 5% exchange between the boron moieties on the cluster and reducing agent[35] and here (Fig. 4b) a similar exchange is observed with benzaldehyde. Whereas with the Al and In systems no such exchange between the group 13 moieties is observed.

In our previous paper, we explored a range of possible intermediates for the reaction of [**1**]$^{2-}$ with a model carbonyl compound, H_2C=O[35]. Here, we extend these studies to include the Al and In analogues using the more realistic benzaldehyde as a model, with the aim of identifying key features that underpin the differences in reactivity observed in the previous section. Specifically, we focus on the reactions of the clusters with the benzaldehyde, and explore how differences in the nature of the E–Pn and E–O bonds influence the ability of the cluster to bind carbonyl functionalities. In the computational experiments we use Me to model the *i*Bu groups on the Al centres, but the ligands are otherwise as described in the crystallographic data (all calculated coordinates can be found in Supplementary Data 1). Selected bond lengths and Gibbs energies for the addition of one and two equivalents of benzaldehyde to [**1**]$^{2-}$, [(Me$_2$Al)P$_7$]$^{2-}$, [(Me$_2$Al)As$_7$]$^{2-}$, [(Me$_2$Ga)P$_7$]$^{2-}$ and [**4**]$^{2-}$ are summarized in Table 3. The values of ΔG shown in the Table correspond to the sequential free energies of benzaldehyde binding: [**X**]$^{2-}$ + C_6H_5CHO→[**X**]$^{2-}$•C_6H_5CHO (first row for each cluster) and [**X**]$^{2-}$•C_6H_5CHO + C_6H_5CHO→[**X**]$^{2-}$•2C_6H_5CHO (second row). The Pn–E and Pn–O bond lengths are also summarized in Table 3. We note that the approximate C_S symmetry of the double adduct [**2**]$^{2-}$•2C_6H_5CHO, is fully consistent with the 2:1:1:1:2 ratio noted in the NMR experiments of [**6**]$^{2-}$. In each case the binding of C_6H_5CHO involves the formation of new Pn–C and E–O bonds with simultaneous cleavage of a Pn–E bond and the π component of a C=O double bond. If we regard the Pn–C and C=O double bonds as approximately constant (at least for the P_7-containing clusters), the trends in free energy should then reflect the difference between the bond energies of the E–P and E–O bonds. Binding of the first molecule of benzaldehyde to the aluminium cluster [(Me$_2$Al)P$_7$]$^{2-}$ is clearly thermodynamically favourable (more so than the corresponding reaction with the boron cluster, [**1**]$^{2-}$), while the free energy for binding the second is close to zero, consistent with [**5**]$^{2-}$ and [**6**]$^{2-}$ being in equilibrium. The change of pnictogen, from P to As ([(Me$_2$Al)P$_7$]$^{2-}$ to [(Me$_2$Al)As$_7$]$^{2-}$) has negligible impact on the equilibria, but the heavier group 13 element In binds benzaldehyde much less strongly with both reactions in Table 3 being endergonic. The relative affinities of the different clusters for benzaldehyde appear, therefore, to correlate with catalytic activity for CO_2 reduction shown in Table 1 (Al > B > In). The structural trends in the mono-adducts offer some insight into the origin of these striking differences in energetics. If we compare the Al adduct to its In analogue, the E–P bond length increases from 2.45 Å to 2.60 Å (Δr = 0.15 Å), while the E–O bond length increases from 1.79 Å to 2.12 Å (Δr = 0.33 Å). This pattern suggests that the strength of the E–O bond is affected more by the change from E = Al to E = In than is the E–P bond, and this rather low affinity of indium for the hard alkoxide ligand (a well-established trend in p-block chemistry) leads to the weaker binding of benzaldehyde in the case of [**4**]$^{2-}$. The greater oxophilicity of the Al-functionalized cluster compared to the indium analogue is consistent with the tendency to bind two molecules of benzaldehyde observed in the experiments, and also with the strong dependence of product distribution on the order of addition observed for the Al systems but not for In. Although a Ga-functionalized cluster could not be cleanly synthetically accessed and tested, the computed benzaldehyde binding affinities for [(Me$_2$Ga)P$_7$]$^{2-}$ suggest that its catalytic competency should be intermediate between those of the In- and Al-functionalized systems.

The mono-benzaldehyde adduct [**2**]$^{2-}$•C_6H_5CHO (identified as [**5**]$^{2-}$ in the NMR experiments) is an aluminium alkoxide species, and there have been numerous computational investigations of the catalytic performance of such species in borohydride reduction of carbonyl groups. Li and co-workers have explored the HBpin hydroboration of CO_2 using a range of aluminium hydride species, based on a cycle of C=O insertion into an Al–H bond to form a formyl species followed by *trans*-metallation to regenerate the hydride along with the product, HCO_2Bpin[51]. By adopting the same fundamental steps, we propose a possible mechanism starting from [(Me$_2$Al)P$_7$]$^{2-}$ in Fig. 5, the full free-energy surface for the same pathway is shown in the supplementary information, Fig. S119. At the level of theory used here, the overall free-

https://doi.org/10.1038/s41467-024-54277-z

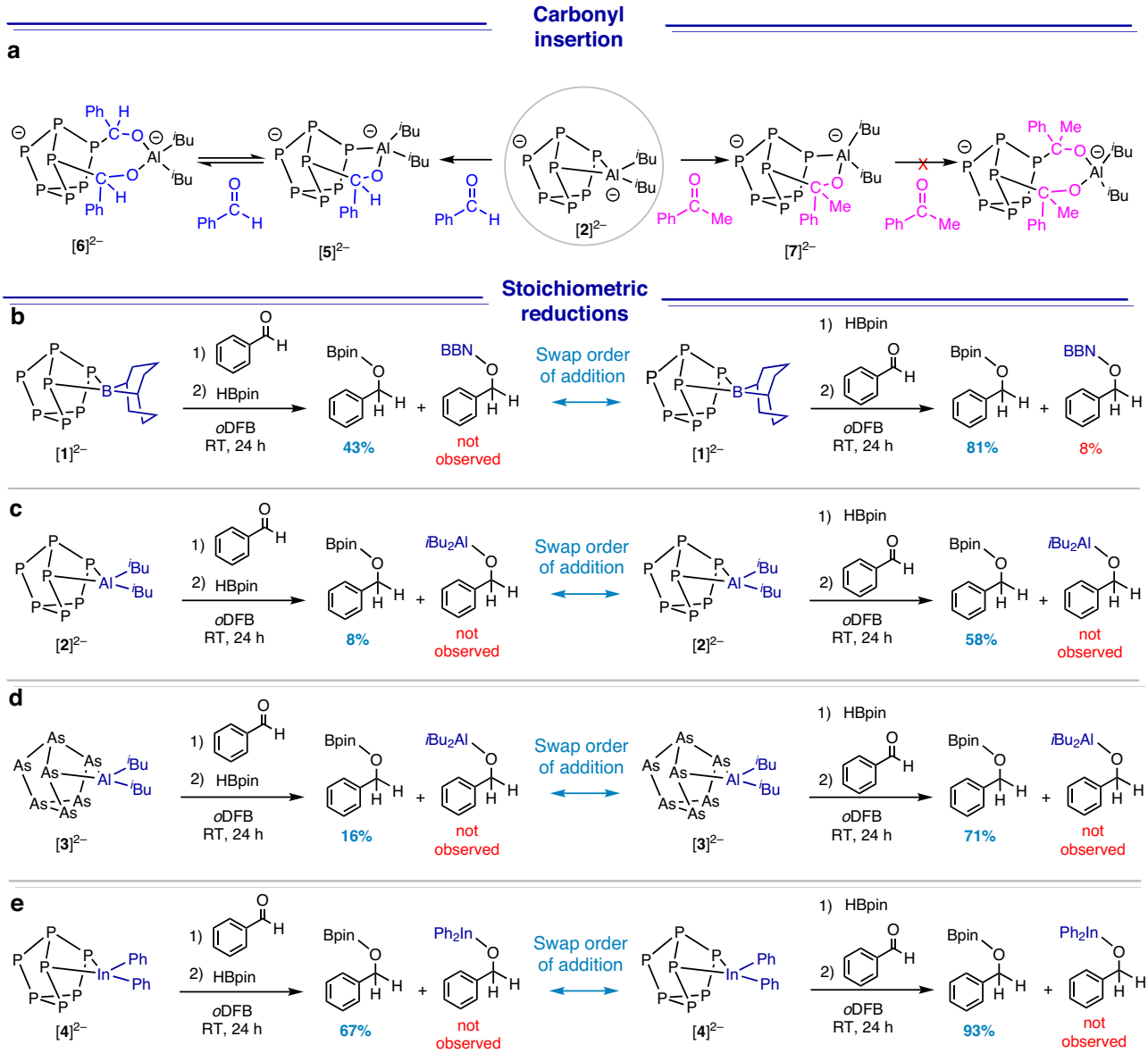

Fig. 4 | Experimental mechanistic studies. a Insertion of carbonyls into the P–Al bond in $[\mathbf{2}]^{2-}$. **b** Stoichiometric reduction of benzaldehyde using $[\mathbf{1}]^{2-}$. **c** Stoichiometric reduction of benzaldehyde using $[\mathbf{2}]^{2-}$. **d** stoichiometric reduction of benzaldehyde using $[\mathbf{3}]^{2-}$. **e** stoichiometric reduction of benzaldehyde using $[\mathbf{4}]^{2-}$.

energy change for the reaction, $C_6H_5CHO + HBPin \rightarrow C_6H_5CH_2O{-}BPin$ is −25.2 kcal/mol. The initial stages of the reaction involve the binding of one and then two benzaldehyde molecules to form the adducts $[(Me_2Al)P_7]^{2-}{\bullet}C_6H_5CHO$ and $[(Me_2Al)P_7]^{2-}{\bullet}2C_6H_5CHO$ discussed above (which correspond to the experimentally observed species, $[\mathbf{5}]^{2-}$ and $[\mathbf{6}]^{2-}$, respectively). The negligible free-energy change for the binding of the second benzaldehyde means that $[(Me_2Al)P_7]^{2-}{\bullet}C_6H_5CHO$ and $[(Me_2Al)P_7]^{2-}{\bullet}2C_6H_5CHO$ are in equilibrium, and an excess of HBpin can trap the former to generate the aluminium hydride intermediate **I1** through *trans*-metallation. In Fig. 5 **I1** is generated by the insertion of the B–H bond into the remaining Al–P bond of $[(Me_2Al)P_7]^{2-}{\bullet}C_6H_5CHO$, although it is also possible that it inserts into the Al–O bond, leaving the $AlMe_2H$ unit anchored to the $[P_7]$ cluster. With the hydride generated, a cycle based on the repeated insertion of C_6H_5CHO (ΔG = +5.2 kcal/mol) followed by *trans*-metallation with HBpin (ΔG = −30.4 kcal/mol) to release the product and regenerate the hydride. The sum of these final two steps is −25.2 kcal/mol, the overall free energy of the reaction. We note that this scheme represents an adaptation of the one in our previous paper dealing exclusively with the boron catalyst, $[\mathbf{1}]^{2-}$, where we proposed that the HBpin inserted into the P–C bond in $[\mathbf{1}]^{2-}{\bullet}C_6H_5CHO$ rather than the E–P bond, as suggested in Fig. 5[34]. The detection of the double addition product, $[\mathbf{6}]^{2-}$, in the case of Al highlights the relative weakness of the remaining Al–P bond in [**5**] and this encouraged us to revise our original proposal, such that it is the E–P, rather than P–C bond that can break to accommodate the H[B] reducing agent.

Herein the synthesis of a family of group 13 functionalized $[Pn_7]$ Zintl clusters is presented. This series of clusters was then systematically explored in their catalytic performance in mediating CO_2 reduction. In terms of TOFs, the performance decreases in the order: $[\kappa^2\text{-}(i\text{Bu}_2\text{Al})P_7]^{2-} > [\kappa^2\text{-}(i\text{Bu}_2\text{Al})As_7]^{2-} > [\kappa^2\text{-}(\text{BBN})P_7]^{2-} > [\kappa^2\text{-}(\text{Ph}_2\text{In})P_7]^{2-}$. Determined to be the most active catalyst, under optimised conditions $[Na(18c6)]_2[\kappa^2\text{-}(i\text{Bu}_2\text{Al})P_7]$ at 0.01 mol% gave a high TON of 9600, and high TOF of 741 h^{-1} with 0.1 mol% at 60 °C. Comparison of $[Na(18c6)]_2[\kappa^2\text{-}(i\text{Bu}_2\text{Al})P_7]$ with other homogenous main group catalyst under similar conditions in this transformation revealed it to be highly competitive, where it even outperformed numerous homogenous transition metal-based catalysts. The $[Na(18c6)]_2[\kappa^2\text{-}(i\text{Bu}_2\text{Al})P_7]$ cluster

https://doi.org/10.1038/s41467-024-54277-z

Table 3 | Calculated free energies (kcal/mol) for the addition of one and two molecules of benzaldehyde to $[X]^{2-}$ and selected bond lengths (Å)

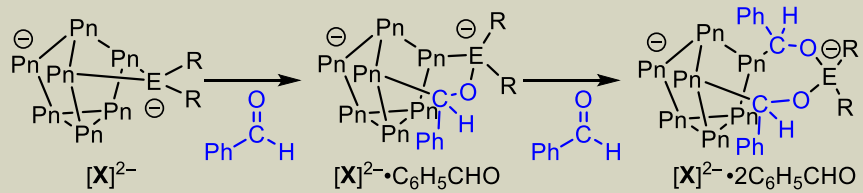

	E–Pn (Å)	Pn–C (Å)	E–O (Å)	ΔG (kcal/mol)
$[\mathbf{1}]^{2-}$	2.09			
$[\mathbf{1}]^{2-} + C_6H_5CHO \rightarrow [\mathbf{1}]^{2-}\bullet C_6H_5CHO$	2.11	1.95	1.48	−11.5
$[\mathbf{1}]^{2-}\bullet C_6H_5CHO + C_6H_5CHO \rightarrow [\mathbf{1}]^{2-}\bullet 2C_6H_5CHO$		1.95	1.51	+1.1
$[(Me_2Al)P_7]^{2-}$	2.45			
$[(Me_2Al)P_7]^{2-} + C_6H_5CHO \rightarrow [(Me_2Al)P_7]^{2-}\bullet C_6H_5CHO$	2.44	1.96	1.79	−13.6
$[(Me_2Al)P_7]^{2-}\bullet C_6H_5CHO + C_6H_5CHO \rightarrow [(Me_2Al)P_7]^{2-}\bullet 2C_6H_5CHO$		1.96	1.79	−1.8
$[(Me_2Al)As_7]^{2-}$	2.55			
$[(Me_2Al)As_7]^{2-} + C_6H_5CHO \rightarrow [(Me_2Al)As_7]^{2-}\bullet C_6H_5CHO$	2.54	2.10	1.79	−12.0
$[(Me_2Al)As_7]^{2-}\bullet C_6H_5CHO + C_6H_5CHO \rightarrow [(Me_2Al)As_7]^{2-}\bullet 2C_6H_5CHO$		2.11	1.79	−2.7
$[\mathbf{4}]^{2-}$	2.63			
$[\mathbf{4}]^{2-} + C_6H_5CHO \rightarrow [\mathbf{4}]^{2-}\bullet C_6H_5CHO$	2.57	1.98	2.13	+4.2
$[\mathbf{4}]^{2-}\bullet C_6H_5CHO + C_6H_5CHO \rightarrow [\mathbf{4}]^{2-}\bullet 2C_6H_5CHO$		1.95	2.13	+13.8
$[(Me_2Ga)P_7]^{2-}$	2.47			
$[(Me_2Ga)P_7]^{2-} + C_6H_5CHO \rightarrow [(Me_2Ga)P_7]^{2-}\bullet C_6H_5CHO$	2.43	1.97	1.91	−2.0
$[(Me_2Ga)P_7]^{2-}\bullet C_6H_5CHO + C_6H_5CHO \rightarrow [(Me_2Ga)P_7]^{2-}\bullet 2C_6H_5CHO$		1.97	1.90	+10.3

https://doi.org/10.1038/s41467-024-54277-z

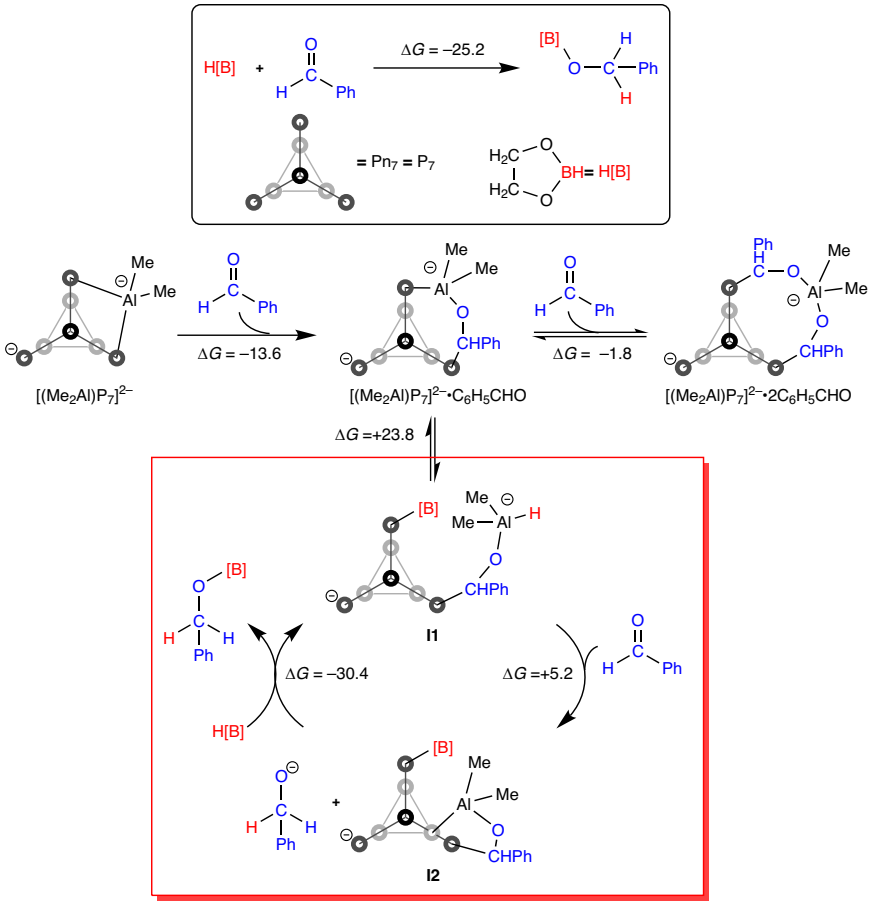

Fig. 5 | Proposed catalytic cycle in which the bis-inserted carbonyl product $[X]^{2-}$•$2C_6H_5CHO$ is off-cycle. The red box shows the catalytic cycle. ΔG change in Gibbs Free Energy. All energies are given in kcal/mol.

was found to be robust and could be recovered from the reaction mixture and recycled several times without loss in performance. Further experimental and computational investigations found a bis-carbonyl inserted species as an off-cycle product, and the determined kinetic isotope effect data was consistent with the H–B hydride being part of a slow step. The factors that direct the differences observed in catalytic competency are complex, and comprehensive mechanistic investigations are still ongoing. However, this work takes a detailed look at how tuning structural features at seven-atom pnictogen clusters modulates catalytic performance in CO_2 reduction chemistry, and further affirms the utility of transition metal-free Zintl clusters in important synthetic transformations.

Methods

Provided here are key protocols

Complete experimental details (general considerations, synthesis & characterization data, catalytic reactions, reactivity studies, kinetics measurements) and further computational details are provided in the Supplementary Information.

Synthesis of $[Na(18c6)]_2[\kappa^2\text{-}(iBu_2Al)P_7]$ ($[2]^{2-}$)

To a Schlenk flask charged with a stir bar and $[Na(18c6)]_2[HP_7]$ (250 mg, 0.32 mmol, 1 equiv.), THF (5 mL) was added and cooled to −30 °C forming a slurry. A solution of diisopropyl aluminium hydride (45 mg, 0.32 mmol. 1 equiv.) in THF (5 mL) was cooled to −30 °C and dropwise added to the $[Na(18c6)]_2[HP_7]$ slurry. Gas evolution was observed, and the reaction was allowed to react for 5 min at −30 °C, after which it was warmed to RT. The mixture was filtered yielding a clear dark orange solution. The solvent was removed under reduced pressure, and the residue was washed with toluene (2 × 20 mL). The residue was dissolved in THF and filtered again, yielding a dark orange solution. Removal of volatiles under reduced pressure yielded glassy orange solids. Isolated Yield: 187 mg, 63%.

Synthesis of $[K(18c6)]_2[\kappa^2\text{-}(iBu_2Al)As_7]$ ($[3]^{2-}$)

To a Schlenk flask charged with a stir bar and $[K(18c6)]_2[HAs_7]$ (250 mg, 0.22 mmol. 1 equiv.), THF (5 mL) was added and cooled to −30 °C forming a slurry. A solution of diisopropal aluminium hydride (31 mg, 0.22 mmol. 1 equiv.) in THF (5 mL) was cooled to −30 °C and dropwise added to the $[K(18c6)]_2[HAs_7]$ slurry. Gas evolution was observed, and the reaction was allowed to react for 5 min at −30 °C, after which it was warmed to RT. The mixture was filtered yielding a black solution. The solvent was removed under reduced pressure, and the residue was washed with toluene (2 × 20 mL). The residue was dissolved in THF and filtered again, yielding a black solution. Removal of volatiles under reduced pressure yielded dark brown solids. Isolated Yield: 101 mg, 71%.

General procedure for carbon dioxide hydroboration

To a J Young NMR tube C_6Me_6, HBBN dimer (36 mg, 0.15 mmol), and a solution of catalysts (with mol % relative to HBBN monomer) in *o*DFB:toluene (0.6 mL, 1:1) were added. The reaction mixture was degassed, and the headspace was refilled with CO_2 (1 atm). The reaction was monitored by ^1H, ^{11}B, and $^{11}B\{^1H\}$ NMR spectroscopy. The NMR conv. was calculated by integration of the crude ^1H NMR spectrum using the C_6Me_6 as an internal standard (^1H δ = 2.20 ppm).

Computational methodology

All density functional theory calculations were performed using the ORCA 5.0.4 programme[52]. All calculations were performed using the r2SCAN-3c method[53], which is based on the r2SCAN functional[54], a bespoke mTZVPP basis set, and D4 and geometrical counterpoise (gCP) corrections[55,56]. The influence of the solvent was modelled using the CPCM model with the following parameters for oDFB: Dielectric Constant (ε) = 14.26 and Refractive Index (n) = 1.443[57,58]. All free energies include a concentration-induced correction of 1.89 kcal/mol to account for the change in standard state from gas phase (1 atm) to solution (1 mol/L)[59].

Data availability

All data generated in this study are provided in Supplementary Information and Supplementary Data 1 and 2. The X-ray crystallographic coordinates for structures reported in this study have been deposited at the Cambridge Crystallographic Data Centre, under deposition numbers 2365860 ([Na(18c6)]$_2$[**2**]) and 2365861 ([K(18c6)]$_2$[**3**]). These data can be obtained free of charge from The Cambridge Crystallographic Data Centre via www.ccdc.cam.ac.uk/data_request/cif. All data are available from the corresponding author upon request.

References

1. Hansen, J. et al. Earth's energy imbalance: confirmation and implications. *Science* **308**, 1431–1435 (2005).
2. Yoro, K. O., Daramola, M. O. Chapter 1 - CO_2 emission sources, greenhouse gases, and the global warming effect. *In*: Advances in Carbon Capture (eds. Rahimpour, M. R., Farsi, M., Makarem, M. A.). Woodhead Publishing (2020).
3. Zhang, X., Zhang, G., Song, C. & Guo, X. Catalytic conversion of carbon dioxide to methanol: current status and future perspective. *Front. Energy Res.* **8**, 621119 (2021).
4. Dalena, F. et al. Chapter 1 - methanol production and applications: an overview. *In*: *Methanol* (eds Basile, A., Dalena, F.). Elsevier (2018).
5. Bertau, M., Offermanns, H., Plass, L., Schmidt, F., Wernicke, H.-J. Methanol: the basic chemical and energy feedstock of the future. Springer (2014).
6. Mondal, U. & Yadav, G. D. Methanol economy and net zero emissions: critical analysis of catalytic processes, reactors and technologies. *Green. Chem.* **23**, 8361–8405 (2021).
7. Song, C. Global challenges and strategies for control, conversion and utilization of CO_2 for sustainable development involving energy, catalysis, adsorption and chemical processing. *Catal. Today* **115**, 2–32 (2006).
8. Mac Dowell, N., Fennell, P. S., Shah, N. & Maitland, G. C. The role of CO2 capture and utilization in mitigating climate change. *Nat. Clim. Change* **7**, 243–249 (2017).
9. Iwarere, S. A., Ramjugernath, D. Carbon dioxide to energy: killing two birds with one stone. In: *Energy Engineering* (eds Raghavan, K. V., Ghosh, P.). Springer Singapore (2017).
10. Goeppert, A., Czaun, M., Jones, J.-P., Surya Prakash, G. K. & Olah, G. A. Recycling of carbon dioxide to methanol and derived products – closing the loop. *Chem. Soc. Rev.* **43**, 7995–8048 (2014).
11. Ganji, P., Chowdari, R. K. & Likozar, B. Photocatalytic reduction of carbon dioxide to methanol: carbonaceous materials, kinetics, industrial feasibility, and future directions. *Energy Fuels* **37**, 7577–7602 (2023).
12. Porosoff, M. D., Yan, B. & Chen, J. G. Catalytic reduction of CO_2 by H_2 for synthesis of CO, methanol and hydrocarbons: challenges and opportunities. *Energy Environ. Sci.* **9**, 62–73 (2016).
13. Onishi, N. & Himeda, Y. CO_2 hydrogenation to methanol by organometallic catalysts. *Chem. Catal.* **2**, 242–252 (2022).
14. Navarro-Jaén, S. et al. Highlights and challenges in the selective reduction of carbon dioxide to methanol. *Nat. Rev. Chem.* **5**, 564–579 (2021).
15. Biswal, T., Shadangi, K. P., Sarangi, P. K. & Srivastava, R. K. Conversion of carbon dioxide to methanol: a comprehensive review. *Chemosphere* **298**, 134299 (2022).
16. Jiang, X., Nie, X., Guo, X., Song, C. & Chen, J. G. Recent advances in carbon dioxide hydrogenation to methanol via heterogeneous catalysis. *Chem. Rev.* **120**, 7984–8034 (2020).
17. Yaroshevsky, A. A. Abundances of chemical elements in the earth's crust. *Geochem. Int.* **44**, 48–55 (2006).
18. Armor, J. N. A history of industrial catalysis. *Catal. Today* **163**, 3–9 (2011).
19. Berger, O., Winters, K. R., Sabourin, A., Dzyuba, S. V. & Montchamp, J.-L. On the cost of academic methodologies. *Org. Chem. Front.* **6**, 2095–2108 (2019).
20. Ludwig, J. R. & Schindler, C. S. Catalyst: sustainable catalysis. *Chem* **2**, 313–316 (2017).
21. Hu, Z., Lu, Y., Liu, M., Zhang, X. & Cai, J. Crystalline red phosphorus for selective photocatalytic reduction of CO_2 into CO. *J. Mat. Chem. A* **9**, 338–348 (2021).
22. Ou, H. et al. Atomically dispersed Au-assisted C–C coupling on red phosphorus for CO_2 photoreduction to C_2H_6. *J. Am. Chem. Soc.* **144**, 22075–22082 (2022).
23. Zhai, R. et al. A review of phosphorus structures as CO_2 reduction photocatalysts. *Small* **19**, 2207840 (2023).
24. Fung, C.-M., Er, C.-C., Tan, L.-L., Mohamed, A. R. & Chai, S.-P. Red phosphorus: an up-and-coming photocatalyst on the horizon for sustainable energy development and environmental remediation. *Chem. Rev.* **122**, 3879–3965 (2022).
25. Zhang, L. et al. Structure and properties of violet phosphorus and its phosphorene exfoliation. *Angew. Chem. Int. Ed.* **59**, 1074–1080 (2020).
26. Ruck, M. et al. Fibrous red phosphorus. *Angew. Chem. Int. Ed.* **44**, 7616–7619 (2005).
27. Zhou, Y., Elliott, S. R. & Deringer, V. L. Structure and bonding in amorphous red phosphorus. *Angew. Chem. Int. Ed.* **62**, e202216658 (2023).
28. Poovan, F., Chandrashekhar, V. G., Natte, K. & Jagadeesh, R. V. Synergy between homogeneous and heterogeneous catalysis. *Catal. Sci. Technol.* **12**, 6623–6649 (2022).
29. Mehta, M. Zintl clusters as catalytic tools for synthesis. *Trends Chem.* **6**, 349–351 (2024).
30. Townrow, O. P. E., Chung, C., Macgregor, S. A., Weller, A. S. & Goicoechea, J. M. A neutral heteroatomic Zintl cluster for the catalytic hydrogenation of cyclic alkenes. *J. Am. Chem. Soc.* **142**, 18330–18335 (2020).
31. Townrow, O. P. E., Duckett, S. B., Weller, A. S. & Goicoechea, J. M. Zintl cluster supported low coordinate Rh(i) centers for catalytic H/D exchange between H_2 and D_2. *Chem. Sci.* **13**, 7626–7633 (2022).
32. Willeit, N. S., Klein, W., Coburger, P., Fritz-Langhals, E. & Fässler, T. F. Functionalised [Ge_9Ni] clusters as homogeneous single-site catalysts for olefin isomerisation reactions. *ChemCatChem* **16**, e202301200 (2024).
33. Poitiers, N. E., Giarrana, L., Huch, V., Zimmer, M. & Scheschkewitz, D. Exohedral functionalization vs. core expansion of siliconoids with group 9 metals: catalytic activity in alkene isomerization. *Chem. Sci.* **11**, 7782–7788 (2020).
34. Wang, Y. et al. Site-selective CO_2 reduction over highly dispersed Ru-SnO_x sites derived from a [$Ru@Sn_9$]$^{6-}$ Zintl cluster. *ACS Catal.* **10**, 7808–7819 (2020).
35. van IJzendoorn, B. et al. A Zintl cluster for transition metal-free catalysis: C=O bond reductions. *J. Am. Chem. Soc.* **144**, 21213–21223 (2022).
36. van IJzendoorn, B., Whittingham, J. B. M., Whitehead, G. F. S., Kaltsoyannis, N. & Mehta, M. A robust Zintl cluster for the catalytic reduction of pyridines, imines and nitriles. *Dalton Trans.* **52**, 13787–13796 (2023).

37. Knapp, C., Zhou, B., Denning, M. S., Rees, N. H. & Goicoechea, J. M. Reactivity studies of group 15 Zintl ions towards homoleptic post-transition metal organometallics: a 'bottom-up' approach to bimetallic molecular clusters. *Dalton Trans.* **39**, 426–436 (2010).
38. Turbervill, R. S. P. & Goicoechea, J. M. Studies on the reactivity of group 15 Zintl ions with carbodiimides: synthesis and characterization of a heptaphosphaguanidine dianion. *Chem. Commun.* **48**, 1470–1472 (2012).
39. Turbervill, R. S. P. & Goicoechea, J. M. Hydropnictination reactions of carbodiimides and isocyanates with protonated heptaphosphide and heptaarsenide Zintl ions. *Eur. J. Inorg. Chem.* **2014**, 1660–1668 (2014).
40. Rahm, M., Hoffmann, R. & Ashcroft, N. W. Atomic and ionic radii of elements 1–96. *Chem. Eur. J.* **22**, 14625–14632 (2016).
41. van IJzendoorn, B. & Mehta, M. Frontiers in the solution-phase chemistry of homoatomic group 15 zintl clusters. *Dalton Trans.* **49**, 14758–14765 (2020).
42. Kostera, S., Peruzzini, M. & Gonsalvi, L. Recent advances in metal catalyst design for CO_2 hydroboration to C1 derivatives. *Catalysts* **11**, 58 (2021).
43. Kepp, K. P. A quantitative scale of oxophilicity and thiophilicity. *Inorg. Chem.* **55**, 9461–9470 (2016).
44. Burés, J. A simple graphical method to determine the order in catalyst. *Angew. Chem. Int. Ed.* **55**, 2028–2031 (2016).
45. Nielsen, C. D. T. & Burés, J. Visual kinetic analysis. *Chem. Sci.* **10**, 348–353 (2019).
46. Vijjamarri, S., O'Denius, T. M., Yao, B., Kubátová, A. & Du, G. Highly selective hydroboration of carbonyls by a manganese catalyst: insight into the reaction mechanism. *Organometallics* **39**, 3375–3383 (2020).
47. Ghatak, T., Makarov, K., Fridman, N. & Eisen, M. S. Catalytic regeneration of a Th–H bond from a Th–O bond through a mild and chemoselective carbonyl hydroboration. *Chem. Commun.* **54**, 11001–11004 (2018).
48. Chong, C. C., Hirao, H. & Kinjo, R. Metal-free σ-bond metathesis in 1,3,2-diazaphospholene-catalyzed hydroboration of carbonyl compounds. *Angew. Chem. Int. Ed.* **54**, 190–194 (2015).
49. Jobbins, W. D., van IJzendoorn, B., Vitorica-Yrezabal, I. J., Whitehead, G. F. S. & Mehta, M. Reactivity of tetrel functionalized heptapnictogen clusters towards heteroallenes. *Dalton Trans.* **52**, 2384–2391 (2023).
50. van IJzendoorn, B., Vitorica-Yrezabal, I., Whitehead, G. & Mehta, M. Heteroallene capture and exchange at functionalised heptaphosphane clusters. *Chem. Eur. J.* **28**, e202103737 (2021).
51. Li, C.-Q., Leng, G. & Li, W. Hydroboration of carbon dioxide with pinacolborane catalyzed by various aluminum hydrides: a comparative mechanistic study. *Cat. Sci. Tech.* **12**, 6129–6141 (2022).
52. Neese, F. Software update: the ORCA program system—version 5.0. *WIREs Comput. Mol. Sci.* **12**, e1606 (2022).
53. Grimme, S., Hansen, A., Ehlert, S. & Mewes, J.-M. r2SCAN-3c: a "swiss army knife" composite electronic-structure method. *J. Chem. Phys.* **154**, 064103 (2021).
54. Furness, J. W., Kaplan, A. D., Ning, J., Perdew, J. P. & Sun, J. Accurate and numerically efficient r2SCAN meta-generalized gradient approximation. *J. Phys. Chem. Lett.* **11**, 8208–8215 (2020).
55. Caldeweyher, E. et al. A generally applicable atomic-charge dependent london dispersion correction. *J. Chem. Phys.* **150**, 154122 (2019).
56. Kruse, H. & Grimme, S. A geometrical correction for the inter- and intra-molecular basis set superposition error in Hartree-Fock and density functional theory calculations for large systems. *J. Chem. Phys.* **136**, 154101 (2012).
57. Barone, V. & Cossi, M. Quantum calculation of molecular energies and energy gradients in solution by a conductor solvent model. *J. Phys. Chem. A* **102**, 1995–2001 (1998).
58. Laurence, C., Nicolet, P., Dalati, M. T., Abboud, J.-L. M. & Notario, R. The empirical treatment of solvent-solute interactions: 15 years of π*. *J. Phys. Chem.* **98**, 5807–5816 (1994).
59. Bursch, M., Mewes, J.-M., Hansen, A. & Grimme, S. Best-practice DFT protocols for basic molecular computational chemistry. *Angew. Chem. Int. Ed.* **61**, e202205735 (2022).

Acknowledgements

We thank the EPSRC and UKRI for funding (EP/V012061/1, EP/Y037391/1, and iCAT CDT EP/S023755/1) and supporting M.M., B.v.I., and W.D.J. We also thank Gareth Smith for mass spectrometric analyses, Anne Davies and Martin Jennings for elemental analyses, and Ralph Adams and Coral Mycroft for NMR spectroscopic enquiries. S.F.A. acknowledges the Saudi government for a postgraduate scholarship.

Author contributions

B.v.I. performed all synthetic synthesis and kinetic work, and subsequent analysis and interpretation, with experiments designed in collaboration with M.M., B.v.I., and W.D.J. performed experimental mechanistic studies. S.F.A. and J.E.M. performed the computational mechanistic studies. B.v.I. and G.F.S.W. performed single crystal XRD analysis. B.v.I. wrote the initial drafts of the manuscript and supplementary information with contributions and edits from J.E.M. and M.M.

Competing interests

The authors declare no competing interests.

Additional information

Supplementary information The online version contains supplementary material available at https://doi.org/10.1038/s41467-024-54277-z.

Correspondence and requests for materials should be addressed to John E. McGrady or Meera Mehta.

Peer review information *Nature Communications* thanks Xijun Liu and the other, anonymous, reviewer(s) for their contribution to the peer review of this work. A peer review file is available.